ACS APPLIED MATERIALS & INTERFACES

Research Article

www.acsami.org

Cotton Wool Derived Carbon Fiber Aerogel Supported Few-Layered $MoSe_2$ Nanosheets As Efficient Electrocatalysts for Hydrogen Evolution

Youfang Zhang,[†] Lizeng Zuo,[†] Longsheng Zhang,[†] Yunpeng Huang,[†] Hengyi Lu,[†] Wei Fan,*[,‡] and Tianxi Liu*[,†,‡]

[†]State Key Laboratory of Molecular Engineering of Polymers, Department of Macromolecular Science, Fudan University, 220 Handan Road, Shanghai 200433, P. R. China

[‡]State Key Laboratory of Modification of Chemical Fibers and Polymer Materials, College of Materials Science and Engineering, Donghua University, 2999 North Renmin Road, Shanghai 201620, P. R. China

Supporting Information

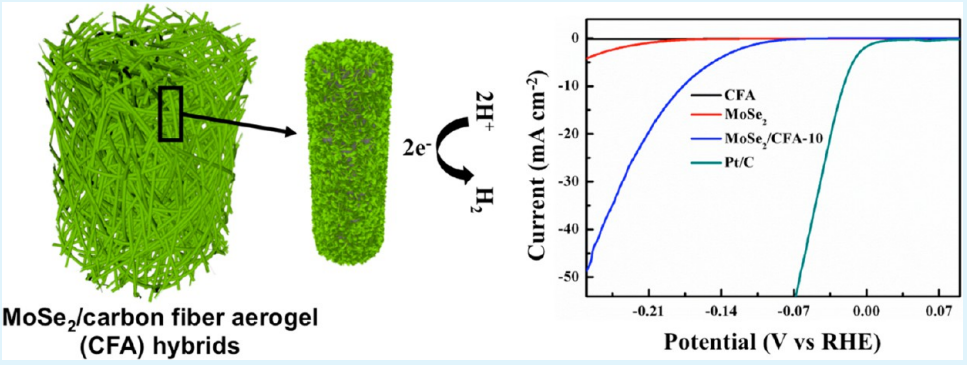

ABSTRACT: Recent studies have proven that newly emerging two-dimensional molybdenum diselenide ($MoSe_2$) is a promising noble-metal-free electrocatalyst for hydrogen evolution reaction (HER). Increasing the exposures of the active edges of $MoSe_2$ nanostructures is a key issue to fully realize the excellent electrochemical properties of $MoSe_2$. In this work, a few-layered $MoSe_2$/carbon fiber aerogel (CFA) hybrids have been facilely obtained through the combination of high-temperature carbonization and one-pot solvothermal reaction. CFA derived from cotton wool is used as a three-dimensional conductive network for construction of hierarchical $MoSe_2$/CFA hybrids, where few-layered $MoSe_2$ nanosheets are uniformly and perpendicularly decorated on the surfaces of CFA. In the designed and prepared hybrids, CFA effectively increases the exposures of the active edges of $MoSe_2$ nanosheets as well as provides reduced lengths for both electron transportation and ion diffusion. Therefore, the obtained optimal $MoSe_2$/CFA hybrid exhibits excellent electrochemical activity as HER electrocatalyst with a small onset potential of −0.104 V vs reversible hydrogen electrode and a small Tafel slope of 62 mV per decade, showing its great potential as a next-generation Pt-free electrocatalyst for HER.

KEYWORDS: *$MoSe_2$, cotton wool, carbon fiber aerogel, electrocatalyst, hydrogen evolution reaction*

1. INTRODUCTION

Hydrogen, a clean renewable energy source, has been vigorously proposed as the promising future energy carrier in the hydrogen-economy paradigm.[1−5] Recently, the generation of hydrogen by efficiently splitting water initiated either by light or electricity has attracted a great deal of attention due to its cleanliness and low cost.[6−16] Hydrogen evolution reaction (HER) is the essential step in water electrolysis where hydrogen is produced by reduction of protons. Both efficient and economical electrocatalysts for HER are required to achieve high current densities at low overpotentials. Although some precious metals and their alloys, such as Pt and Pd, have exhibited high catalytic activity for HER, the high cost and low natural abundance restrict their practical applications in industrial production of hydrogen.[17] Recently, two-dimensional (2D) earth-abundant and low-cost transition metal chalcogenides (TMDs), such as MoS_2, $MoSe_2$, WS_2, and WSe_2, have been extensively investigated due to their excellent electrocatalytic performance for HER.[18−27] Among them, $MoSe_2$ is a newly emerging catalyst owing to its low cost, high chemical stability, and excellent electrocatalytic activity.[28−32] Similar with the catalytic mechanism of MoS_2, the electrocatalytic HER activity of $MoSe_2$ depends strongly on its active selenium edge sites, while its basal planes were catalytically inert.[33] Therefore,

Received: December 29, 2015
Accepted: February 29, 2016
Published: February 29, 2016

DOI: 10.1021/acsami.5b12772
ACS Appl. Mater. Interfaces 2016, 8, 7077−7085

reducing the size of $MoSe_2$ down to nanoscale and increasing the exposures of its active edges can boost the catalytic activities of $MoSe_2$. It is reported that the vertically aligned $MoSe_2$ molecular layers on curved and rough surfaces such as Si nanowires and carbon microfibers possess maximally exposed active edge sites, and thereby exhibit large exchange current densities in HER.[21] In addition to the exposure of active edge sites, electrical conductivity is another key factor influencing the HER performance. However, the poor conductivity between two adjacent van der Waals bonded layers of $MoSe_2$ would significantly suppress their overall HER rate. In this regard, preparation of uniformly distributed $MoSe_2$ nanostructures with more exposed selenium edges on a conductive substrate is an effective strategy to enhance its electrocatalytic performance for HER.

Carbon materials, including graphene, carbon nanotubes (CNTs), carbon nanofibers (CNFs), activated carbon, carbon aerogels (CAs), and carbon fiber cloth, etc., are ideal substrates for loading $MoSe_2$ to improve its electrocatalytic activity,[34−39] owing to the unique physicochemical properties and excellent conductivity of these carbon materials. For example, Yang et al. found that $MoSe_2$ nanosheets grown on graphene exhibit abundant catalytic edge sites and excellent electrical coupling to the underlying graphene network, resulting in relatively low onset potentials of −0.15 V vs RHE and 0.05 V vs RHE.[40] $MoSe_2$ nanosheets/carbon fiber cloth hybrids have also been prepared, in which ultrathin and defect-rich $MoSe_2$ nanosheet arrays were grown on carbon fiber cloth. The carbon fiber matrix could decrease the charge transfer resistance of $MoSe_2$-based catalysts during HER process because the charges could be transferred from highly conductive carbon fiber directly to active edge sites of each single layer of $MoSe_2$ nanosheets, thus enhancing the electrocatalytic performance for HER.[34] However, most of the stacked layers are parallel to the conductive substrates, but the utilization of three-dimensional (3D) substrates with interconnected frameworks have rarely been reported.

Among various carbon materials, CAs have been extensively investigated due to their 3D interconnected networks and outstanding properties, such as low density, highly continuous porosity, good electrical conductivity, and chemical inertness.[37,41−43] Generally, there are three types of CAs, including organic-derived CAs carbonized in inert atmosphere,[44−46] graphene or CNTs-based aerogels fabricated by chemical vapor deposition or self-gelation,[47−49] and biomass-derived CAs synthesized from nature materials.[50,51] Among these three types of CAs, biomass-derived CAs have received considerable attention in recent years owing to their rich source, low cost, nontoxicity, and renewability.[52] Different biomass sources, such as watermelon, winter melon, bacterial cellulose, etc., are utilized to prepare CAs by freeze-drying or supercritical carbon dioxide drying processes to prevent pore collapse. However, these production processes are complicated and time-consuming, thus restricting their further application. In comparison, CAs can be synthesized directly from the carbonization of cotton wool without any complicated drying treatment, where cotton wool is cheap, abundant, and sustainable, making it a promising raw material for fabrication of CAs.[41] To the best of our knowledge, the nanocomposites of $MoSe_2$ nanosheets and CFA have not been previously applied in the field of HER.

Herein, lightweight and porous carbon fiber aerogels (CFAs) are facilely produced using cotton wools as the raw materials, and further employed as 3D networks for in situ growth of few-layered $MoSe_2$ nanosheets. The specific fiber structure of CFAs can form 3D interconnected frameworks, which could not only prevent the aggregation of $MoSe_2$ nanosheets, but also facilitate ion diffusion and charge transportation during the electrocatalytic process. Morphology characterizations show that few-layered $MoSe_2$ nanosheets are perpendicularly decorated on the rough and curved surface of CFAs, maximizing the exposure of highly active edge sites. As a consequence, the optimized $MoSe_2$/CFA hybrid exhibits excellent electrocatalytic performance with lower onset potential and smaller Tafel slope compared to that of pure $MoSe_2$ nanosheets, making it a promising catalyst for HER.

2. EXPERIMENTAL SECTION

2.1. Materials. Cotton wool was purchased from Shanghai Hygienic Materials Co. Ltd. Selenium powder (Se, 99.99%), sodium molybdat dihydrat (Na_2MoO_4) (99.99%) and hydrazine hydrate ($N_2H_4{\cdot}H_2O$, 50 wt % in water) were obtained from Sinopharm Chemical Reagent Co. Ltd. Pt/C catalyst (20 wt % platinum on carbon black) was purchased from Alfa Aesar. *N*,*N*-dimethylformamide (DMF) was obtained from Shanghai Chemical Reagent Company. All chemicals were analytic grade and used without further purification. Deionized (DI) water was used as the solvent throughout the experiments.

2.2. Preparation of Carbon Fiber Aerogel (CFA). Cotton wool was carbonized in a tubular furnace under nitrogen atmosphere at 800 °C for 2 h with a heating rate of 5 °C min^{-1}. After the furnace cooled down to room temperature naturally, the CFA was obtained.

2.3. Preparation of $MoSe_2$/CFA Hybrids. The preparation of $MoSe_2$/CFA hybrids is shown in Scheme 1. $MoSe_2$/CFA hybrids with various mass loading of $MoSe_2$ were synthesized by a one-pot solvothermal reaction method. Briefly, 90 mg selenium powder were dispersed in 30 mL hydrazine hydrate at 80 °C for 1 h via continuous stirring to obtain 3 mg mL^{-1} Se solution. Meanwhile, 30 mg CFA and a certain amount of Na_2MoO_4 were added in 15 mL DMF. Afterward, 5 mL of Se solution was dropwise added into the above DMF solution with the final Mo/Se molar ratio of 1:2. Finally, the mixture was transferred into a 40 mL Teflon stainless-steel autoclave and reacted at 180 °C for 12 h, and then cooled to room temperature naturally. The resulting products were collected by a tweezer and subsequently washed with DI water several times. The final products were obtained after drying at 80 °C for 6 h, and subsequently annealing at 450 °C for 2 h with a ramping rate of 5 °C min^{-1} under N_2 atmosphere to improve the crystallinity of $MoSe_2$ nanosheets. The $MoSe_2$/CFA hybrids with 5, 10, and 15 mL Se solution (3 mg/mL) were obtained finally and denoted as $MoSe_2$/CFA-5, $MoSe_2$/CFA-10, and $MoSe_2$/

Scheme 1. Preparation of $MoSe_2$/CFA Hybrids

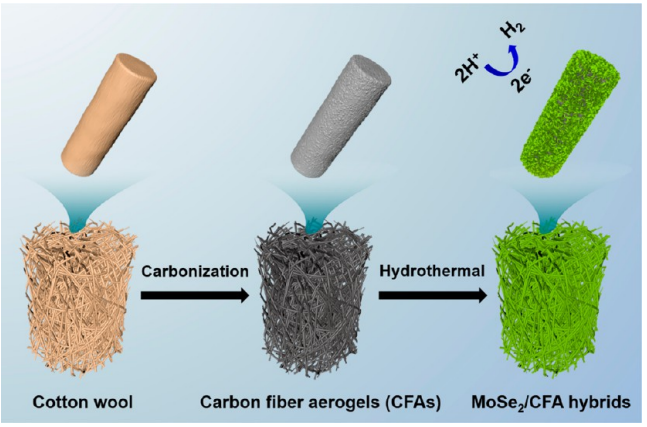

DOI: 10.1021/acsami.5b12772
ACS Appl. Mater. Interfaces 2016, 8, 7077−7085

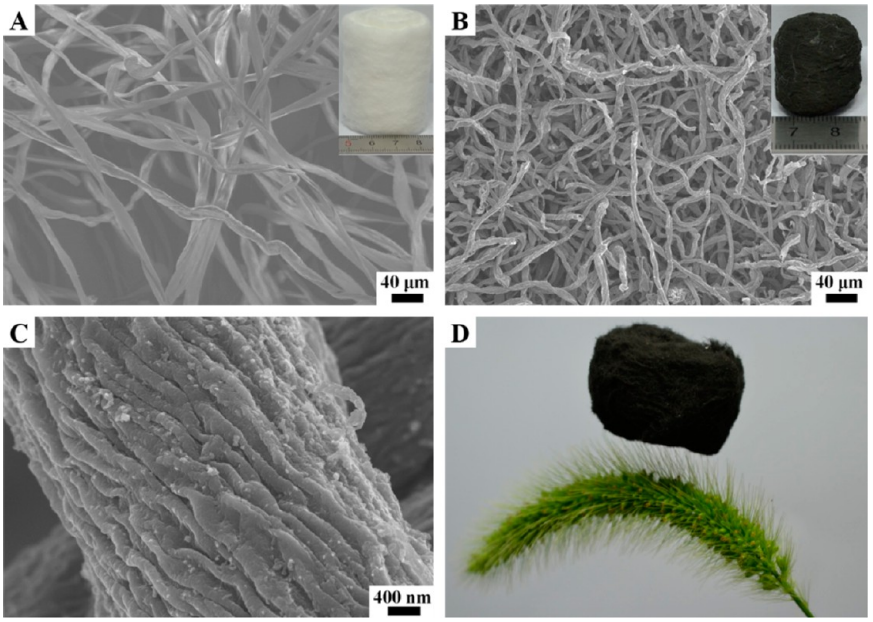

Figure 1. FESEM images of cotton wool (A), CFA at low (B), and high (C) magnifications, and the digital photograph of a CFA on a green bristle grass (D). The inset in A is the digital photograph of a cylindrical cotton wool, and the inset in B is the digital photograph of a CFA.

CFA-15, respectively. For comparison, pure $MoSe_2$ nanosheets were also prepared by the same procedure without the addition of CFA.

2.4. Characterization. The structure and morphology of the as-prepared samples were characterized by field emission scanning electron microscopy (FESEM) (Ultra 55, Zeiss) at an acceleration voltage of 5 kV, and the chemical composition was investigated by the energy dispersive X-ray spectroscopy (EDX). The specific surface area and pore size distribution of CFA were characterized with a belsorp-max surface area detecting instrument (Tristar3000) by N_2 physisorption at 77 K. The crystalline structure of the obtained products was characterized using powder X-ray diffraction (XRD) with 2θ ranging from 5° to 80° on an X'Pert Pro X-ray diffractometer with CuKα radiation (λ = 0.1542 nm) under a voltage of 40 kV and a current of 40 mA. Raman spectra were measured on LabRam-1B French Dilor Com (λ_{ex} = 532 nm). X-ray photoelectron spectroscopy (XPS) analyses were made with a VG ESCALAB 220I-XL device. All XPS spectra were corrected using C 1s line at 284.6 eV. Thermogravimetric analysis (Pyris 1 TGA) was performed under air flow from 100 to 700 °C at a heating rate of 10 °C min^{-1}.

2.5. Electrochemical Measurements. Prior to all hydrogen evolution performance measurements, glass carbon electrodes (GCE) were pretreated according to the previously reported method.[41] The hydrogen evolution performance tests were carried out in 0.5 M H_2SO_4 aqueous electrolyte solution at room temperature using a typical three electrode cells (Pt wire as counter electrode, a saturated calomel electrode as the reference electrode, and the sample modified GCE as the working electrode). Typically, the working electrode was prepared as follows. Four mg of $MoSe_2$/CFA hybrids was dispersed in 2 mL of a mixed DMF/water solution (a volume ratio of 1:1) containing 20 μL 5 wt % nafion by at least 30 min sonication to form a homogeneous suspension. Afterward, 10 μL of the above solution (20 μg $MoSe_2$/CFA hybrids) was dropped onto GCE, and finally the electrode was dried.

All electrochemical studies were performed with a CHI 660D electrochemical workstation (Chenhua Instruments Co, Shanghai, China) in a standard three-electrode setup at room temperature. The potential was calibrated to reversible hydrogen electrode (RHE) by adding a value of (0.241 + 0.059 pH) V for all the electrochemical tests. The electrocatalytic activity of $MoSe_2$/CFA composite catalysts toward HER was examined using liner sweep voltammetry (LSV) in nitrogen purged 0.5 M H_2SO_4 with a scan rate of 2 mV s^{-1} at room temperature. The onset potential was determined based on the beginning of linear regime in the Tafel plot, and no *iR* compensation was applied for all the electrochemical measurements in 0.5 M H_2SO_4. Electrochemical impedance spectroscopy (EIS) measurements were carried out in 0.5 M H_2SO_4 from 0.01 Hz to 100 kHz at the potential of 200 mV with amplitude of 5 mV.

3. RESULTS AND DISCUSSION

3.1. Morphology and Structure of $MoSe_2$/CFA Hybrids. Black and lightweight carbon fiber aerogels were obtained by carbonization of white raw cotton wool under nitrogen atmosphere. As shown, the inset in Figure 1A,B, the diameter and the height of the cylindrical cotton wool are 3.0 and 4.4 cm, while the diameter and the height of the CFA decreased to 1.8 and 2.0 cm. In other words, the volume of the CFA is only 16.4% of that of the raw cotton wool. SEM image of the raw cotton wool (Figure 1A) shows that the raw cotton wool is rich in fibers with different diameters ranging from tens of nanometers to several micrometers. These long fibers are irregularly twisted and form a porous and interconnected 3D network. After pyrolysis, the CFA shows a similar fiber structure with a small shrinkage of the fiber diameter as compared with raw cotton wool (Figure 1B). By zooming in a single fiber, it is interesting and worth noting that the surface of the fibers is full of wrinkles and gullies (Figure 1C), which could offer more active regions for the growth of $MoSe_2$ and greatly prevent the aggregation of $MoSe_2$ nanosheets. In contrast, the surface of the fibers of raw cotton wool is rather smooth as shown in Figure S1. Additionally, the weight of CFA is 160.1 mg, only about 10% of that of the cotton wool (1454.9 mg) before carbonization. Due to the high porosity and lightweight, the obtained CFA can stand on a green bristle grass, which is shown in Figure 1D. Therefore, CFA would be the potential template for further growth of $MoSe_2$ nanosheets. Besides, BET data were further investigated by nitrogen isothermal adsorption. The specific surface area of CFA is 62.0 m^2 g^{-1}. As shown in Figure S2A, there is a clear hysteresis loop in the isotherm curve of CFA and this curve belongs to type IV, indicating that there are a lot of meso-pores in CFA.

DOI: 10.1021/acsami.5b12772
ACS Appl. Mater. Interfaces 2016, 8, 7077−7085

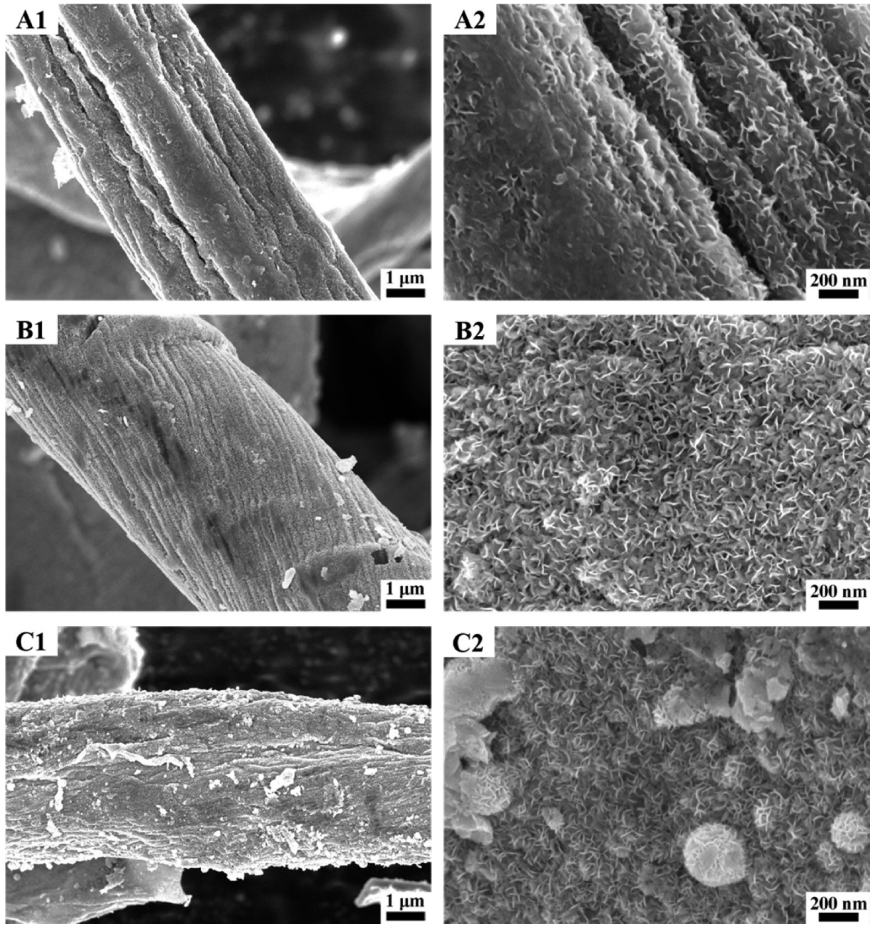

Figure 2. FESEM images of $MoSe_2$/CFA-5 hybrid (A1 and A2), $MoSe_2$/CFA-10 hybrid (B1 and B2), and $MoSe_2$/CFA-15 hybrid (C1 and C2).

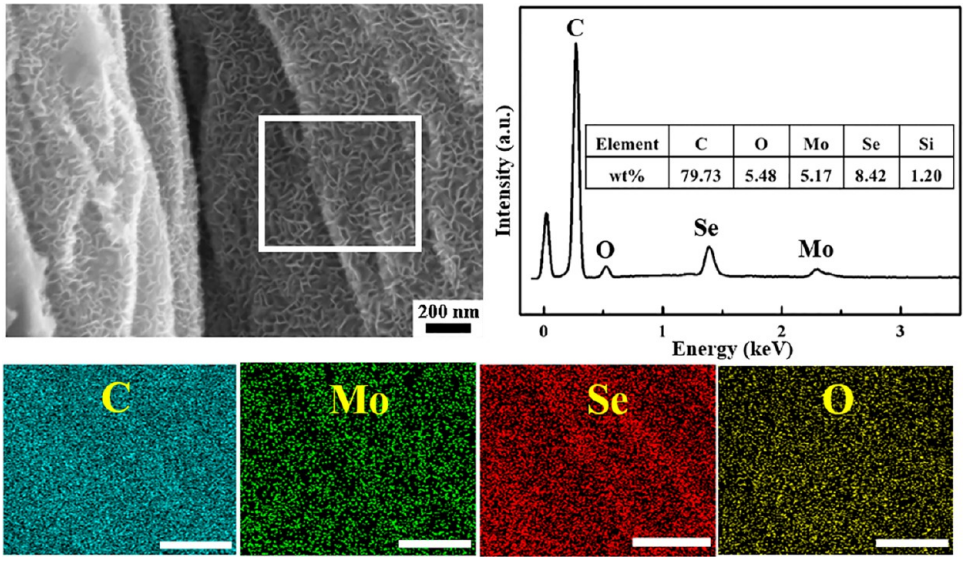

Figure 3. EDX mapping of $MoSe_2$/CFA-10 hybrid (Scale bar: 250 nm).

Moreover, from the pore size distribution curve (Figure S2B), it can be seen that the pore size distribution of CFA shows a relatively narrow distribution centered at 4 nm, which is in the meso-porous range.

The morphology of $MoSe_2$/CFA hybrids with different loading amount of $MoSe_2$ nanosheets was investigated by SEM observation. As shown in Figure 2, $MoSe_2$ nanosheets are sparsely interspersed on the surface of CFA for $MoSe_2$/CFA-5 hybrid (Figure 2A1,A2). With the initial selenium dosage increased to 30 mg, ultrathin $MoSe_2$ nanosheets are uniformly anchored on the surface of CFA for $MoSe_2$/CFA-10 hybrid as displayed in Figure 2B. The obvious ripples and corrugations can be observed in the SEM images at high magnifications (Figure 2B2), suggesting the ultrathin nature of the $MoSe_2$

DOI: 10.1021/acsami.5b12772
ACS Appl. Mater. Interfaces 2016, 8, 7077−7085

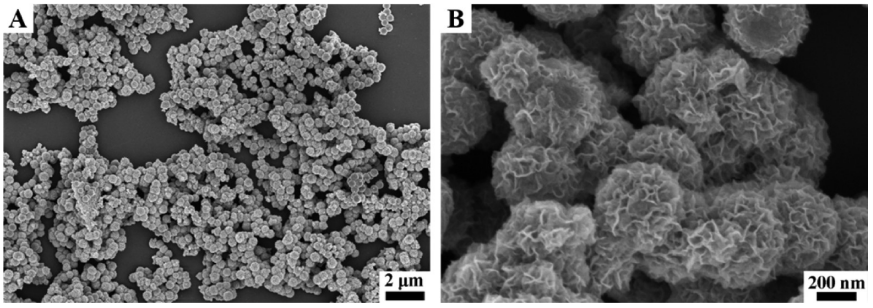

Figure 4. FESEM images of pure $MoSe_2$ at low (A) and high (B) magnifications.

nanosheets. However, with further increasing the dosage of selenium, excess $MoSe_2$ nanosheets tend to aggregate into microsized spheres on the surface of CFA, which would decrease the exposure of active edge sites of $MoSe_2$ nanosheets (Figure 2C1,C2). Therefore, the reasonable amount of CFA can effectively prevent the aggregation of $MoSe_2$ nanosheets as well as offer a 3D open structure that is beneficial for fast hydrogen evolution. The EDX mapping analysis of $MoSe_2$/CFA-10 hybrid (Figure 3) proves the coexistence and homogeneous dispersion of C, Mo, and Se elements, further confirming that $MoSe_2$ nanosheets are distributed evenly on the fiber framework in CFA. Besides, the weight ratio of Mo element and Se element on the surface of fiber framework in CFA is about 5.17% and 8.42%, corresponding to the Mo to Se molar ratio of about 1 to 2. In contrast, as shown in Figure 4, pure $MoSe_2$ nanosheets prepared by solvothermal reaction without adding CFA disorderly aggregated into large microsized spheres.

Figure 5 shows the XRD patterns of the as-prepared CFA, pure $MoSe_2$ and $MoSe_2$/CFA-10 hybrid. As for CFA sample,

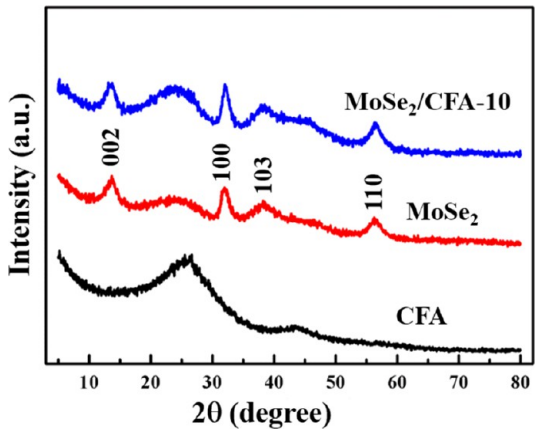

Figure 5. XRD patterns of pure $MoSe_2$ nanosheets, CFA, and $MoSe_2$/CFA-10 hybrid.

the wide significant peak centered at $2\theta = 26°$ and a weak peak at $2\theta = 44°$ can be assigned to the (002) and (100) planes (JCPDS No. 01-0646), respectively, indicating that the obtained CFA possesses a low degree of crystallinity. For the annealed pure $MoSe_2$ and $MoSe_2$/CFA-10 hybrid, all of the XRD peaks can be readily indexed to the hexagonal $MoSe_2$ phase (JPCDS No. 29-0914). As shown in Figure 5, $MoSe_2$/CFA-10 hybrid shows sharp peaks at $2\theta = 13.6°$, 32.0°, 38.2°, and 56.5°, which can be well indexed to the (002), (100), (103), and (110) diffraction planes of $MoSe_2$, respectively. Additionally, a weak and wide diffraction peak at $2\theta = 26°$ for CFA can be observed in the pattern of $MoSe_2$/CFA-10 hybrid. Therefore, the XRD results also suggest that $MoSe_2$ nanosheets are successfully grown on the surface of CFA. Besides, the formation of $MoSe_2$/CFA hybrids can be further confirmed by Raman analysis. As exhibited in Figure S3, the Raman spectrum displays two prominent peaks of CFA and two main peaks of $MoSe_2$. The peaks located at 1344 and 1606 cm^{-1} respectively correspond to the D and G bands of typical carbon materials, while the characteristic peaks located at 237 and 284 cm^{-1} correspond to out-of-plane mode of A_{1g} and in-plane mode of E^1_{2g} for $MoSe_2$ in the hybrid.

XPS spectra are investigated to analyze the chemical state of Mo and Se in the $MoSe_2$/CFA-10 hybrid. As shown in Figure 6A, the survey scan indicates that C, Mo, Se, and O elements coexist in $MoSe_2$/CFA-10 hybrid. The peak of C 1s spectrum is centered at 284.5 eV, which corresponds to sp^2 C. High resolution Mo 3d spectrum (Figure 6B) shows characteristic peaks located at 232.0 and 228.9 eV corresponding to the binding energies of Mo $3d_{3/2}$ and Mo $3d_{5/2}$, respectively, suggesting the dominance of Mo (IV) in the MoS_2/CFA samples. In the high resolution Se 3p and Se 3d spectrum shown in Figure 6C,D, the binding energies of Se $3d_{5/2}$ and Se $3d_{3/2}$ at 54.3 and 55.2 eV, along with Se $3p_{3/2}$ and Se $3p_{1/2}$ at 160.8 and 166.4 eV, respectively, all indicate the oxidation chemical state of Se^{2-}. These results are consistent with those reported previously for $MoSe_2$. Besides, TGA data are investigated to analyze the loading amounts of $MoSe_2$ in the $MoSe_2$/CFA hybrids. As calculated from Figure S4, the content of $MoSe_2$ in the hybrids is 8.4%, 16.0%, and 25.1% for $MoSe_2$/CFA-5, $MoSe_2$/CFA-10, and $MoSe_2$/CFA-15 hybrids, respectively.

3.2. Electrochemical Performance of $MoSe_2$/CFA Hybrids. The electrocatalytic performace of $MoSe_2$/CFA hybrids for HER were investigated in a typical three-electrode electrochemical cell setup with 0.5 M H_2SO_4 solution. Before all the measurements, cyclic voltammogram (CV) tests were first performed about 20 cycles in order to stabilize the catalysts. In addition, the polarization curves and Tafel plots were taken at a scan rate of 2 mV s^{-1}. From Figure 7, it can be observed that $MoSe_2$/CFA-10 hybrid shows a smaller onset overpotential of −0.104 V vs RHE than that of the other two $MoSe_2$/CFA hybrids ($MoSe_2$/CFA-5 hybrid and $MoSe_2$/CFA-15 hybrid). Furthermore, $MoSe_2$/CFA-10 hybrid exhibits a current density of 10 mA cm^{-2} at a lower overpotential of 0.179 V, which is much smaller than those of $MoSe_2$/CFA-5 hybrid (10 mA cm^{-2} at 0.257 V) and $MoSe_2$/CFA-15 hybrid (10 mA cm^{-2} at 0.199 V). All these results suggest that the $MoSe_2$/CFA-10 hybrid exhibits the optimal electrocatalytic activity for hydrogen evolution. As mentioned above, $MoSe_2$/CFA-10 hybrid shows the optimized hierarchical structure with uniform

DOI: 10.1021/acsami.5b12772
ACS Appl. Mater. Interfaces 2016, 8, 7077−7085

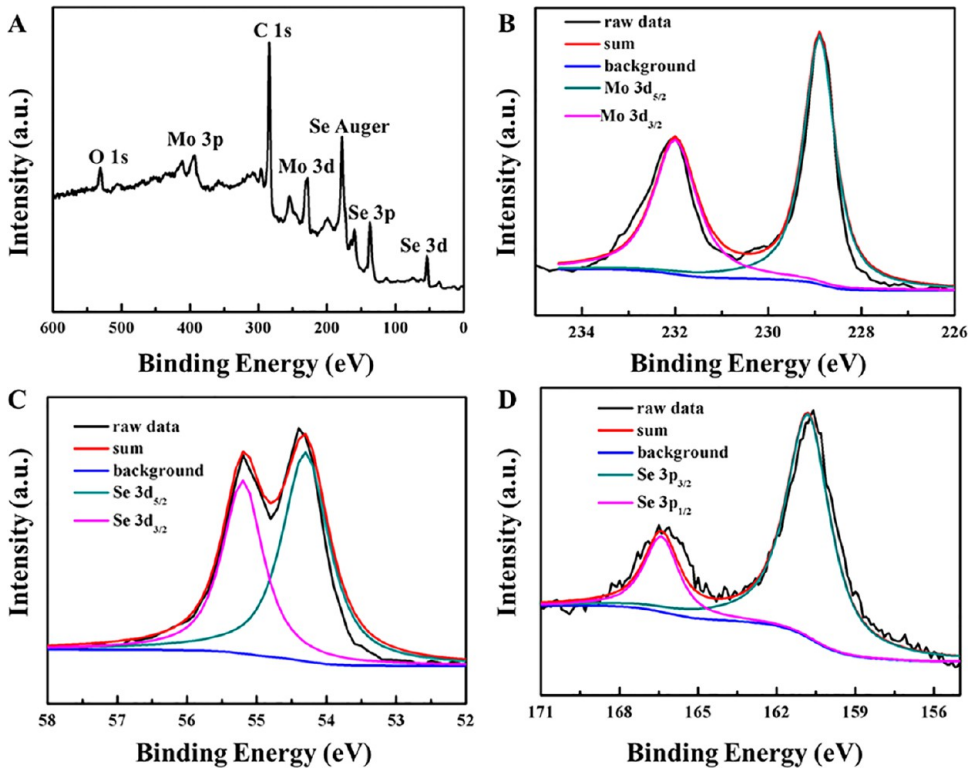

Figure 6. XPS survey spectrum (A), Mo 3d spectrum (B), Se 3p spectrum (C), and Se 3d (D) of $MoSe_2$/CFA-10 hybrid.

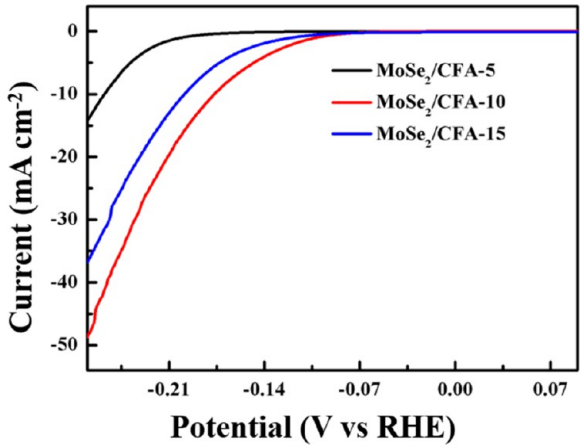

Figure 7. LSV polarization curves for $MoSe_2$/CFA-5 hybrid, $MoSe_2$/CFA-10 hybrid, and $MoSe_2$/CFA-15 hybrid modified GCE in N_2-purged 0.5 M H_2SO_4 solution. Scan rate: 2 mV s^{-1}.

distribution of vertically aligned $MoSe_2$ nanosheets on the surface of CFA and more active edges exposed. In contrast, only sparsely distributed or overloaded $MoSe_2$ nanosheets are observed on the surface of CFA for $MoSe_2$/CFA-5 hybrid and $MoSe_2$/CFA-15 hybrid, respectively, which exhibits less active edges. Therefore, in this regard, $MoSe_2$/CFA-10 hybrid with proper amount of $MoSe_2$ nanosheets shows the optimized HER catalytic activity.

Figure 8A shows the polarization curves of CFA, pure $MoSe_2$, $MoSe_2$/CFA-10 hybrid and commercial available Pt/C catalyst. As presented in Figure 8A, Pt/C modified GCE exhibits extremely high HER catalytic activity with a near zero onset potential and large current density. However, CFA shows almost no HER activity with a near horizontal line within the potential window, which is in accordance with the previous reports for carbon materials.[22,40] Pure $MoSe_2$ nanosheets exhibit poor HER catalytic activity in terms of high onset potential and low current densities owing to its disordered stacking and aggregation. The improved electrocatalytic HER activity for $MoSe_2$/CFA-10 hybrid suggests the synergistic effect between highly conductive CFA and electroactive $MoSe_2$ nanosheets. As mentioned above, the main advantage of using highly porous CFA as the 3D conductive templates is a good balance between the adequate junction active sites for relatively high catalyst loading, the uniform distribution of the nanosized $MoSe_2$, and the excellent conductive interconnected network. First of all, the distinctive twisted cotton based fibers fully filled with wrinkles and gullies are able to offer more anchoring sites for the growth of $MoSe_2$ nanosheets and meanwhile prevent the aggregation of $MoSe_2$ nanosheets, maximizing the exposure of accessible active catalytic sites of $MoSe_2$ nanosheets. Furthermore, vertical growth of $MoSe_2$ nanosheets could significantly decrease the charge transfer resistance during HER process, since the charges could be transferred directly from conductive carbon fibers to each layer of $MoSe_2$ nanosheets, instead of along adjacent stacked layers with an extremely high resistance. Therefore, the $MoSe_2$/CFA-10 hybrid, in which $MoSe_2$ nanosheets exhibit uniform distribution with less aggregation and better interfacial overlaps with the conductive CFA template, shows higher catalytic activity for HER.

A Tafel slope is the inherent property of electrocatalysts, and it is always correlated with reaction pathway and the adsorption type. Therefore, the Tafel slope can be used for quantitative kinetic analysis of HER. Normally, the linear portions of the Tafel plots fit well with Tafel equation ($\eta = b \log(j) + a$, where η is the overpotential, j is the current density, and b is the Tafel slope). The Tafel plots for pure $MoSe_2$, $MoSe_2$/CFA-10 hybrid

DOI: 10.1021/acsami.5b12772
ACS Appl. Mater. Interfaces 2016, 8, 7077−7085

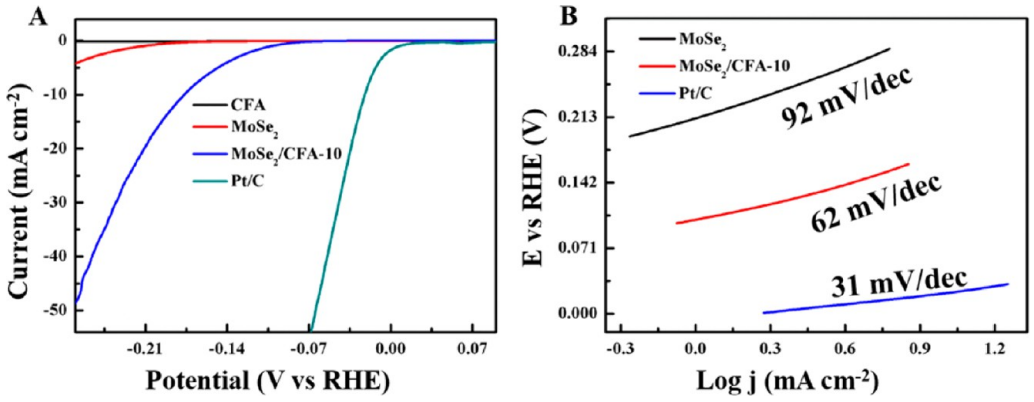

Figure 8. LSV polarization curves (A) for GCE modified with different materials in N_2-purged 0.5 M H_2SO_4 solution. Scan rate: 2 mV s^{-1}. Tafel plots (B) for Pt/C, pure $MoSe_2$, and $MoSe_2$/CFA-10 hybrid modified GCE.

and Pt/C derived from the polarization curves are shown in Figure 8B. The values of Tafel slopes are ~92, ~62, and ~31 mV per decade for pure $MoSe_2$, $MoSe_2$/CFA-10 hybrid, and Pt/C, respectively. Compared to pure $MoSe_2$, the small Tafel slope of $MoSe_2$/CFA-10 hybrid suggests a faster increment of HER rate with increasing the overpotentials. The HER performance of the $MoSe_2$/CFA-10 hybrid is comparable or superior to some MoS_2 or $MoSe_2$ based HER catalysts, as listed in Table S1. Additionally, with the Tafel slope of 62 mV per decade, the HER process of $MoSe_2$/CFA-10 hybrid catalyst follows the Volmer–Heyrovsky or the Volmer–Tafel mechanism with the Volmer reaction as the rate-determining step.

To further investigate the interfacial interactions and electrode kinetics of the $MoSe_2$/CFA hybrids during the HER process, electrochemical impedance spectroscopy (EIS) tests were conducted for pure $MoSe_2$, CFA, and $MoSe_2$/CFA-10 hybrid with an AC amplitude of 5 mV in 0.5 M H_2SO_4 aqueous solution. As shown in Figure 9, the Nyquist plots of

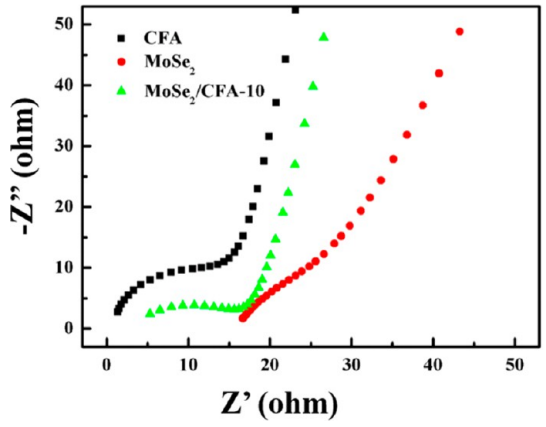

Figure 9. Nyquist plots for CFA, pure $MoSe_2$, and $MoSe_2$/CFA-10 hybrid.

the modified electrodes consist of capacitive semicircles in the high frequency region and straight lines at different constant inclining angles in the low frequency region. In the high frequencies zone, the semicircle is related to the charge transfer resistance (R_{ct}) of H^+ reduction at the electrode–electrolyte interface, and the intersection of the curves at the real axis is related to the solution resistance (R_s). In addition, the constant inclining angle of the straight line refers to ion diffusion resistance in the electrode structure. Obviously, CFA has the smallest R_{ct} and R_s and largest line slop due to its good conductivity, which is beneficial for efficient transport of ions and electrons. Furthermore, R_{ct} and R_s of $MoSe_2$/CFA-10 hybrid is lower than that of pure $MoSe_2$, while the line slope of $MoSe_2$/CFA-10 hybrid is larger than that of pure $MoSe_2$, indicating that the 3D conductive open structure of $MoSe_2$/CFA-10 hybrid significantly decreases the ion and charge transfer resistance along the electrode–electrolyte interface. To evaluate the long-term stability of $MoSe_2$/CFA-10 hybrid modified electrode, CV measurement was carried out continuously for 3000 cycles from −0.4 V to +0.2 V vs RHE at 100 mV s^{-1}, and the LSV curves before and after CV tests were given in Figure 10. The $MoSe_2$/CFA-10 hybrid retains a

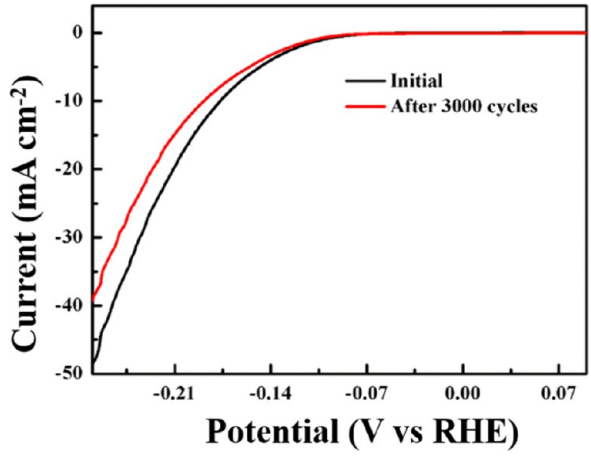

Figure 10. LSV polarization curves for $MoSe_2$/CFA-10 hybrid modified GCE recorded before and after 3000 times of CV cycles.

low onset potential similar to the initial one while the current density slightly reduces after continuous 3000 cycles, indicating its good durability. The slightly reduced current density might be due to the consumption of H^+ and accumulation of H_2 around the electrode surface that hinders the reaction, or the gradual decrease of the active edges.

4. CONCLUSIONS

In summary, a highly active and stable electrocatalyst for hydrogen evolution is successfully developed based on $MoSe_2$/CFA hybrids via the combination of high-temperature carbonization and solvothermal reaction. In this designed hybrid, CFAs with rough surfaces and 3D interconnected network can

DOI: 10.1021/acsami.5b12772
ACS Appl. Mater. Interfaces 2016, 8, 7077–7085

not only uniformly distribute $MoSe_2$ nanosheets to maximize the exposure of its active edges, but also afford a highly conductive skeleton for rapid diffusion of ions and electrons during the HER process. Therefore, the optimal $MoSe_2$/CFA hybrid with well-dispersed and edge-rich $MoSe_2$ nanosheets possesses excellent catalyst performance for HER with low onset potential (−0.104 V vs RHE), small Tafel slope (62 mV per decade), and long-term durability, making it a potential candidate for efficient catalysts in electrochemical hydrogen production.

■ ASSOCIATED CONTENT

Supporting Information

The Supporting Information is available free of charge on the ACS Publications website at DOI: 10.1021/acsami.5b12772.

FESEM image of raw cotton at high magnification, N_2 adsorption−desorption analysis of CFA, Raman spectra of $MoSe_2$/CFA-10 and TGA curves CFA, pure $MoSe_2$, and $MoSe_2$/CFA hybrids (PDF)

■ AUTHOR INFORMATION

Corresponding Authors

*E-mail: weifan@dhu.edu.cn (W.F.).

*Tel: +86-21-55664197. Fax: +86-21-65640293. E-mail: txliu@fudan.edu.cn or txliu@dhu.edu.cn; (T.L.).

Notes

The authors declare no competing financial interest.

■ ACKNOWLEDGMENTS

The authors are grateful for the financial support of the National Natural Science Foundation of China (51125011, 51433001).

■ REFERENCES

(1) Wan, C.; Regmi, Y. N.; Leonard, B. M. Multiple Phases of Molybdenum Carbide as Electrocatalysts for the Hydrogen Evolution Reaction. *Angew. Chem., Int. Ed.* **2014**, *53*, 6407−6410.

(2) Cui, W.; Liu, Q.; Xing, Z. C.; Asiri, A. M.; Alamry, K. A.; Sun, X. P. MoP Nanosheets Supported on Biomass-Derived Carbon Flake: One-Step Facile Preparation and Application as a Novel High-Active Electrocatalyst toward Hydrogen Evolution Reaction. *Appl. Catal., B* **2015**, *164*, 144−150.

(3) Peng, X.; Yan, Y.; Ge, X. M.; Liu, Z. L.; Wang, J. Y.; Wang, X. Investigation of Molybdenum Carbide Nano-rod as an Efficient and Durable Electrocatalyst for Hydrogen Evolution in Acidic and Alkaline Media. *Appl. Catal., B* **2014**, *154−155*, 232−237.

(4) Lin, T. W.; Liu, C. J.; Lin, J. Y. Facile Synthesis of MoS_3/Carbon Nanotube Nanocomposite with High Catalytic Activity toward Hydrogen Evolution Reaction. *Appl. Catal., B* **2013**, *134−135*, 75−82.

(5) Wirth, S.; Harnisch, F.; Weinmann, M.; Schroder, U. Comparative Study of IVB-VIB Transition Metal Compound Electrocatalysts for the Hydrogen Evolution Reaction. *Appl. Catal., B* **2012**, *126*, 225−230.

(6) Hou, D. M.; Zhou, W. J.; Liu, X. J.; Zhou, K.; Xie, J.; Li, G. Q.; Chen, S. W. Pt Nanoparticles/MoS_2 nanosheets/Carbon Fibers as Efficient Catalyst for the Hydrogen Evolution Reaction. *Electrochim. Acta* **2015**, *166*, 26−31.

(7) Tian, J. Q.; Liu, Q.; Cheng, N. Y.; Asiri, A. M.; Sun, X. P. Self-Supported Cu_3 P Nanowire Arrays as an Integrated High-Performance Three-Dimensional Cathode for Generating Hydrogen from Water. *Angew. Chem., Int. Ed.* **2014**, *53*, 9577−9581.

(8) Yan, H. J.; Tian, C. G.; Wang, L.; Wu, A.; Meng, M. C.; Zhao, L.; Fu, H. G. Phosphorus-Modified Tungsten Nitride/Reduced Graphene Oxide as a High-Performance, Non-Noble-Metal Electrocatalyst for the Hydrogen Evolution Reaction. *Angew. Chem., Int. Ed.* **2015**, *54*, 6325−6329.

(9) Moya, A.; Cherevan, A.; Marchesan, S.; Gebhardt, P.; Prato, M.; Eder, D.; Vilateta, J. J. Oxygen Vacancies and Interfaces Enhancing Photocatalytic Hydrogen Production in Mesoporous CNT/TiO_2 Hybrids. *Appl. Catal., B* **2015**, *179*, 574−582.

(10) Lin, T. W.; Liu, C. J.; Dai, C. S. Ni_3S_2/Carbon Nanotube Nanocomposite as Electrode Material for Hydrogen Evolution Reaction in Alkaline Electrolyte and Enzyme-Free Glucose Detection. *Appl. Catal., B* **2014**, *154−155*, 213−220.

(11) Huang, Y. P.; Lu, H. Y.; Gu, H. H.; Fu, J.; Mo, S. Y.; Wei, C.; Miao, Y. E.; Liu, T. X. A CNT@$MoSe_2$ Hybrid Catalyst for Efficient and Stable Hydrogen Evolution. *Nanoscale* **2015**, *7*, 18595−18602.

(12) Shi, Y. F.; Hua, C. X.; Li, B.; Fang, X. P.; Yao, C. H.; Zhang, Y. C.; Hu, Y. S.; Wang, Z. X.; Chen, L. Q.; Zhao, D. Y.; Stucky, G. D. Highly Ordered Mesoporous Crystalline $MoSe_2$ Material with Efficient Visible-Light-Driven Photocatalytic Activity and Enhanced Lithium Storage Performance. *Adv. Funct. Mater.* **2013**, *23*, 1832−1838.

(13) Maitra, U.; Gupta, U.; De, M.; Datta, R.; Govindaraj, A.; Rao, C. N. R. Highly Effective Visible-Light-Induced H_2 Generation by Single-Layer 1T-MoS_2 and a Nanocomposite of Few-Layer 2H-MoS_2 with Heavily Nitrogenated Graphene. *Angew. Chem., Int. Ed.* **2013**, *52*, 13057−13061.

(14) Wang, H. T.; Lu, Z. Y.; Kong, D. S.; Sun, J.; Hymel, T. M.; Cui, Y. Electrochemical Tuning of MoS_2 Nanoparticles on Three-Dimensional Substrate for Efficient Hydrogen Evolution. *ACS Nano* **2014**, *8*, 4940−4947.

(15) Fan, X. Q.; Zhang, L. X.; Wang, M.; Huang, W. M.; Zhou, Y. J.; Li, M. L.; Cheng, R. L.; Shi, J. L. Constructing Carbon-Nitride-Based Copolymers via Schiff Base Chemistry for Visible-Light Photocatalytic Hydrogen Evolution. *Appl. Catal., B* **2016**, *182*, 68−73.

(16) Liu, Q.; Tian, J. Q.; Cui, W.; Jiang, P.; Cheng, N. Y.; Asiri, A. M.; Sun, X. P. Carbon Nanotubes Decorated with CoP Nanocrystals: A Highly Active Non-Noble-Metal Nanohybrid Electrocatalyst for Hydrogen Evolution. *Angew. Chem., Int. Ed.* **2014**, *53*, 6710−6714.

(17) Jiang, P.; Liu, Q.; Liang, Y. H.; Tian, J. Q.; Asiri, A. M.; Sun, X. P. A Cost-Effective 3D Hydrogen Evolution Cathode with High Catalytic Activity: FeP Nanowire Array as the Active Phase. *Angew. Chem., Int. Ed.* **2014**, *53*, 12855−12859.

(18) Wu, Z. Z.; Fang, B. Z.; Bonakdarpour, A.; Sun, A.; Wilkinson, D. P. WS_2 Nanosheets as a Highly Efficient Electrocatalyst for Hydrogen Evolution Reaction. *Appl. Catal., B* **2012**, *125*, 59−66.

(19) Gong, Q. F.; Cheng, L.; Liu, C. H.; Zhang, M.; Feng, Q. L.; Ye, H. L.; Zeng, M.; Xie, L. M.; Liu, Z.; Li, Y. G. Ultrathin $MoS_{2(1-x)}Se_{2x}$ Alloy Nanoflakes for Electrocatalytic Hydrogen Evolution Reaction. *ACS Catal.* **2015**, *5*, 2213−2219.

(20) Balendhran, S.; Walia, S.; Nili, H.; Ou, J. Z.; Zhuuiykov, S.; Kaner, R. B.; Sriam, S.; Bhaskaran, M.; Zadeh, K. Two-Dimensional Molybdenum Trioxide and Dichalcogenides. *Adv. Funct. Mater.* **2013**, *23*, 3952−3970.

(21) Wang, H. T.; Kong, D. S.; Johanes, P.; Cha, J. J.; Zheng, G. Y.; Yan, K.; Liu, N.; Cui, Y. $MoSe_2$ and WSe_2 Nanofilms with Vertically Aligned Molecular Layers on Curved and Rough Surfaces. *Nano Lett.* **2013**, *13*, 3426−3433.

(22) Liao, L.; Zhu, J.; Bian, X. J.; Zhu, L.; Scanlon, M. D.; Girault, H. H.; Liu, B. H. MoS_2 Formed on Mesoporous Graphene as a Highly Active Catalyst for Hydrogen Evolution. *Adv. Funct. Mater.* **2013**, *23*, 5326−5333.

(23) Zhang, J.; Wang, Q.; Wang, L. H.; Li, X. A.; Huang, W. Layer-Controllable WS_2-Reduced Graphene Oxide Hybrid Nanosheets with High Electrocatalytic Activity for Hydrogen Evolution. *Nanoscale* **2015**, *7*, 10391−10397.

(24) Zhang, L.; Wu, H. B.; Yan, Y.; Wang, X.; Lou, X. W. Hierarchical MoS_2 Microboxes Constructed by Nanosheets with Enhanced Electrochemical Properties for Lithium Storage and Water Splitting. *Energy Environ. Sci.* **2014**, *7*, 3302−3306.

(25) Rao, C. N. R.; Ramakrishna Matte, H. S. S.; Maitra, U. Graphene Analogues of Inorganic Layered Materials. *Angew. Chem., Int. Ed.* **2013**, *52*, 13162−13185.

(26) Xie, J. F.; Zhao, H.; Li, S.; Wang, R. X.; Sun, X.; Zhou, M.; Zhou, J. F.; Lou, X. W.; Xie, Y. Defect-Rich MoS_2 Ultrathin Nanosheets with Additional Active Edge Sites for Enhanced Electrocatalytic Hydrogen Evolution. *Adv. Mater.* **2013**, *25*, 5807−5813.
(27) Xu, K.; Wang, F. M.; Wang, Z. X.; Zhan, X. Y.; Wang, Q. S.; Cheng, Z. Z.; Safdar, M.; He, J. Component-Controllable $WS_{2(1-x)}Se_{2x}$ Nanotubes for Efficient Hydrogen Evolution Reaction. *ACS Nano* **2014**, *8*, 8468−8476.
(28) Huang, Y. P.; Miao, Y. E.; Fu, J.; Mo, S. Y.; Wei, C.; Liu, T. X. Perpendicularly Oriented Few-Layer $MoSe_2$ on SnO_2 Nanotubes for Efficient Hydrogen Evolution Reaction. *J. Mater. Chem. A* **2015**, *3*, 16263−16271.
(29) Zhang, Y. J.; Gong, Q. F.; Li, L.; Yang, H. C.; Li, Y. G.; Wang, Q. B. $MoSe_2$ Porous Microspheres Comprising Monolayer Flakes with High Electrocatalytic Activity. *Nano Res.* **2015**, *8*, 1108−1115.
(30) Hu, X. L.; Zhang, W.; Liu, X. X.; Mei, Y. N.; Huang, Y. H. Nanostructured Mo-Based Electrode Materials for Electrochemical Energy Storage. *Chem. Soc. Rev.* **2015**, *44*, 2376−2404.
(31) Shaw, J. C.; Zhou, H. L.; Chen, Y.; Weiss, N. O.; Liu, Y.; Huang, Y.; Duan, X. F. Chemical Vapor Deposition Growth of Monolayer $MoSe_2$ Nanosheets. *Nano Res.* **2014**, *7*, 511−517.
(32) Jia, L. P.; Sun, X.; Jiang, Y. M.; Yu, S. J.; Wang, C. M. A Novel $MoSe_2$ -Reduced Graphene Oxide/Polyimide Composite Film for Applications in Electrocatalysis and Photoelectrocatalysis Hydrogen Evolution. *Adv. Funct. Mater.* **2015**, *25*, 1814−1820.
(33) Xu, S. J.; Lei, Z. Y.; Wu, P. Y. Facile Preparation of 3D MoS_2 /$MoSe_2$ Nanosheet-Graphene Networks as Efficient Electrocatalysts for the Hydrogen Evolution Reaction. *J. Mater. Chem. A* **2015**, *3*, 16337−16347.
(34) Qu, B.; Yu, X. B.; Chen, Y. J.; Zhu, C. L.; Li, C. Y.; Yin, Z. X.; Zhang, X. T. Ultrathin $MoSe_2$ Nanosheets Decorated on Carbon Fiber Cloth as Binder-Free and High-Performance Electrocatalyst for Hydrogen Evolution. *ACS Appl. Mater. Interfaces* **2015**, *7*, 14170−14175.
(35) Mao, S.; Wen, Z. H.; Ci, S. Q.; Guo, X. R.; Ostrikov, K.; Chen, J. H. Perpendicularly Oriented $MoSe_2$/Graphene Nanosheets as Advanced Electrocatalysts for Hydrogen Evolution. *Small* **2015**, *11*, 414−419.
(36) Zhu, Z. L.; Li, M. F.; Xia, M. F.; Wan, J. N.; Zhang, Q. X. Preparation and Characterization of Polymer-Based Spherical Activated Carbons. *Chin. J. Polym. Sci.* **2008**, *26*, 645−651.
(37) Wei, G.; Miao, Y. E.; Zhang, C.; Yang, Z.; Liu, Z. Y.; Tjiu, W. W.; Liu, T. X. Ni-Doped Graphene/Carbon Cryogels and Their Applications as Versatile Sorbents for Water Purification. *ACS Appl. Mater. Interfaces* **2013**, *5*, 7584−7591.
(38) Rafiei, S.; Noroozi, B.; Arbab, S.; Haghi, A. K. Characteristic Assessment of Stabilized Polyacrylonitrile Nanowebs for the Production of Activated Carbon Nano-Sorbents. *Chin. J. Polym. Sci.* **2014**, *32*, 449−457.
(39) Liu, Z. Q.; Li, N.; Zhao, H. Y.; Du, Y. P. Colloidally Synthesized $MoSe_2$ /Graphene Hybrid Nanostructures as Efficient Electrocatalysts for Hydrogen Evolution. *J. Mater. Chem. A* **2015**, *3*, 19706−19710.
(40) Tang, H.; Dou, K. P.; Kaun, C. C.; Kuang, Q.; Yang, S. H. $MoSe_2$ Nanosheets and Their Graphene Hybrids: Synthesis, Characterization and Hydrogen Evolution Reaction Studies. *J. Mater. Chem. A* **2014**, *2*, 360−364.
(41) Bi, H. C.; Yin, Z. Y.; Cao, X. H.; Xie, X.; Tan, C. L.; Huang, X.; Chen, B.; Chen, F. T.; Yang, Q. L.; Bu, X. Y.; Lu, X. H.; Sun, L. T. Carbon Fiber Aerogel Made from Raw Cotton: A Novel, Efficient and Recyclable Sorbent for Oils and Organic Solvents. *Adv. Mater.* **2013**, *25*, 5916−5921.
(42) Cai, H. L.; Sharma, S.; Liu, W. Y.; Mu, W.; Liu, W.; Zhang, X. D.; Deng, Y. L. Aerogel Microspheres from Natural Cellulose Nanofibrils and Their Application as Cell Culture Scaffold. *Biomacromolecules* **2014**, *15*, 2540−2547.
(43) Zhang, Y. F.; Fan, W.; Huang, Y. P.; Zhang, C.; Liu, T. X. Graphene/Carbon Aerogels Derived from Graphene Crosslinked Polyimide as Electrode Materials for Supercapacitors. *RSC Adv.* **2015**, *5*, 1301−1308.
(44) Wang, X.; Lu, L. L.; Yu, Z. L.; Xu, X. W.; Zheng, Y. R.; Yu, S. H. Scalable Template Synthesis of Resorcinol-Formaldehyde/Graphene Oxide Composite Aerogels with Tunable Densities and Mechanical Properties. *Angew. Chem., Int. Ed.* **2015**, *54*, 2397−2401.
(45) Qian, H.; Kucernak, A. R.; Greenhalgh, E. S.; Bismarck, A.; Shaffer, M. S. P. Multifunctional Structural Supercapacitor Composites Based on Carbon Aerogel Modified High Performance Carbon Fiber Fabric. *ACS Appl. Mater. Interfaces* **2013**, *5*, 6113−6122.
(46) Guo, K.; Song, H. H.; Chen, X. H.; Du, X.; Zhong, L. Graphene Oxide as an Anti-Shrinkage Additive for Resorcinol-Formaldehyde Composite Aerogels. *Phys. Chem. Chem. Phys.* **2014**, *16*, 11603−11608.
(47) Tang, G. Q.; Jiang, Z. G.; Li, X. F.; Zhang, H. B.; Dasari, A.; Yu, Z. Z. Three Dimensional Graphene Aerogels and Their Electrically Conductive Composites. *Carbon* **2014**, *77*, 592−599.
(48) Sun, H. Y.; Xu, Z.; Gao, C. Ultra-Flyweight, Synergistically Assembled Carbon Aerogels. *Adv. Mater.* **2013**, *25*, 2554−2560.
(49) Hu, H.; Zhao, Z. B.; Gogotsi, Y.; Qiu, J. H. Compressible Carbon Nanotube-Graphene Hybrid Aerogels with Superhydrophobicity and Superoleophilicity for Oil Sorption. *Environ. Sci. Technol. Lett.* **2014**, *1*, 214−220.
(50) Li, Y. B.; Zhang, H. M.; Liu, P. R.; Wang, Y.; Yang, H. G.; Li, Y.; Zhao, H. J. Self-Supported Bimodal-Pore Structured Nitrogen-Doped Carbon Fiber Aerogel as Electrocatalyst for Oxygen Reduction Reaction. *Electrochem. Commun.* **2015**, *51*, 6−10.
(51) Hao, P.; Zhao, Z.; Tian, J.; Li, H. D.; Sang, Y. H.; Yu, G. W.; Cai, H. Q.; Liu, H.; Wong, C. P.; Umar, A. Hierarchical Porous Carbon Aerogel Derived from Bagasse for High Performance Supercapacitor Electrode. *Nanoscale* **2014**, *6*, 12120−12129.
(52) Xu, X. Z.; Zhou, J.; Nagaraju, D. H.; Jiang, L.; Marinov, V. R.; Lubineau, G.; Alshareef, H. N.; Oh, M. Flexible, Highly Graphitized Carbon Aerogels Based on Bacterial Cellulose/Lignin: Catalyst-Free Synthesis and Its Application in Energy Storage Devices. *Adv. Funct. Mater.* **2015**, *25*, 3193−3202.

DOI: 10.1021/acsami.5b12772
ACS Appl. Mater. Interfaces 2016, 8, 7077−7085